Optimization System for Hydrocyclones Classification and Granulometric Analysis via Mathematical Morphology

Jonathas Jerônimo Barbosa (jonathasbarbosa@gmail.com)
JanKees van der Poel (jkvdoel@yahoo.com.br)
Programa de Pós-Graduação em Engenharia Mecânica, Departamento de Engenharia Mecânica, Universidade Federal da Paraíba
Belarmino Barbosa Lira (belarminoblira@yahoo.com.br)
Departamento de Engenharia Civil e Ambiental, Centro de Tecnologia, Universidade Federal da Paraíba, Secretaria de Integração Universidade Setor Produtivo (SIUSP/UFPB)
Leonardo Vidal Batista (leonardo@di.ufpb.br)
Programa de Pós-Graduação em Engenharia Mecânica, Departamento de Engenharia Mecânica/Departamento de Informática, Universidade Federal da Paraíba

Abstract. *Hydrocyclones are classification devices which divide an ore particle flux in two directions, according to a granulometric threshold. Thus, a hydrocyclone classifies ore particles based on size, ensuring a final product within a required size. Many interdependent variables determine the classification efficiency, including cyclone geometry, operational conditions and characteristics of the ore to be classified. Inadequate settings of these variables result in a wide range of problems, including final product quality reduction, energy waste and low production caused by several cycles of comminution/classification. Optimizing hydrocyclones operation by means of computational simulation techniques requires formulating a mathematical model and acquisition of experimental granulometric distribution data in their exit fluxes. Actually, the most accurate granulometric analysis techniques present some disadvantages, mainly related with high cost of acquisition and maintenance of sophisticated devices. On the other hand, cheaper systems are generally characterized by low precision or long time to conclude the analysis. The only techniques capable to apply a morphological analysis, today considered fundamental to mineral characterization, are image based, generally reached by microscopy. However, morphological analysis made by humans is a hard and time consuming operation. This, in turns, tends to result in mistakes caused by limitations on the operator technical formation and subjectivity related to the process. This work investigates the viability of using computational image analysis techniques to achieve a granulometric profile.*

Keywords: *Mathematical Modelling; Mathematical Morphology; Granulometric Analysis*

1. INTRODUCTION

The massive use of mills and hydrocyclones operating in closed circuit, in various industrial applications of huge socio-economic relevance, gives special importance to the problem of developing mathematical models and processes aiming at this closed circuit optimization (Lira, 1990; Kohmuench, 2000). Applications of hydrocycloning classifiers are vast: sugar, ore, paper, rubber, petrochemical, agricultural and gas industries, civil construction and purification of brackish water, among many others. It is generally considered that hydrocyclones bring a number of advantages over other methods of particle classification: they do not have moving parts, do not damage the environment, they are compact and also they have a low cost of acquisition and operation (Kapur and Meloy, 1998).

Preliminary investigations indicated that the mill-hydrocyclone circuits in important industrial sectors operate with a particle return rate of over 25% from the hydrocyclone to the mill (Lira, 1985). By using appropriate mathematical models for optimizing these circuits, one could reduce this inefficiency to less than 10%. This detected inefficiency leads to an enormous and continuing reduction in productivity, with serious losses for these companies. However, the problem goes beyond profitability reduction: since multiple milling cycles do reflect in unnecessary energy waste and overgrinding, there is in fact the installation of environmental damages. An improvement of this order in the mineral industry will certainlly contribute to an economic heating, with healthy social and environmental consequences.

A practical problem of optimizing the Lynch-Rao Model (Lynch and Rao, 1975) requires obtaining the experimental granulometric distribution (Silva *et al.*, 2004) in the hydrocyclone's discharge and overflow. The empirical granulometric distribution depends on the hydrocyclone's operating characteristics, as well as on the nature and momentary material conditions one wishes to classify. After obtaining the granulometric distribution, it is possible to calculate all necessary constants needed to characterize the classification system, in conformity to the Lynch-Rao Model. In possession of these constants, it is possible to perform computer simulations of the hydrocyclone under new operating conditions, which enables its quick and low cost optimization.

Particle granulometry by laser diffraction is also used in many industrial sectors. The applicable particle range size goes from 0.02 micrometers to 3000 micrometers. This technique is based on the fact that the laser diffraction angle is proportional to the particles' size. Modern equipments implement the Mie Equations (Lira, 1985), which model the interaction between light and matter. The disadvantages of this technique include the high cost of the equipments and the requirement imposed on knowing or on determining the refractive material's indices and also the material and its

surroundings absorption allotment.

The granulometric qualitative analysis by means of manual microscopy is also widely used. However, the operator workload is strenuously, making the result prone to errors caused by factors related to fatigue, operators' training and the subjectivity inherent to the human visual analysis. A visual inspection by humans is particularly limited in the granulometric analysis, which requires the counting of thousands of particles to obtain a statistically significant profile of the material.

Techniques based on technologically sophisticated devices have high costs, mainly associated with equipment purchasing and maintenance and also, in many cases, with problems associated by using ionizing radiation (Gamma and X Rays). Cheaper systems, moreover, often require the use of thermally insulated drying chambers, which means more time to obtain results, and are characterized by low accuracy in determining the granulometric profile. In almost all cases, the analysis time depends on the granulometric range that will be analyzed and on the accuracy required. In other words, the higher the accuracy, the more time is needed for the analysis, which can reach up to 24 hours.

Computerized image analysis, or Computer Vision, has been widely used to characterize particles' size and morphology (Wojnar, 1999). Computer Vision techniques based on Mathematical Morphology are also being increasingly adopted in many sectors (such as pharmaceutical, biotechnology, ceramics, polymers, pigments, abrasives and explosives industries), as they allow further investigation of relevant phenomena such as particle's clustering tendency and impure particles detection.

There are computerized image granulometric analysis commercial systems, as well as there are commercial systems for mill-hydrocyclone circuit optimization based on various mathematical models, but industrial secrets prevent the techniques employed to be disclosed in detail. It is to be noted that a recent study (Dur *et al.*, 2004) showed the existence of a good correlation between laser diffraction granulometry and computer aided image analysis in a problem of fine mineral granulometry, but the cited work employed a non-automatic analysis method — the software is only an assistant to the operator.

The main objective of this paper is concerned with investigating the feasibility on using computational image analysis techniques to obtaining a granulometric profile. This method has the advantages of having no subjectivity when related to the manual microscopy, as well as a reduced cost when compared to the laser diffraction method. The rest of the paper is organized as follows: Section 2 gives a brief description of materials and methods used in this work; Section 3 presents the results obtained by means of computational sieving; and Section 4 discusses and concludes the paper.

2. MATERIALS AND METHODS

This section aims to provide the materials and methods that enabled the realization of this study, as well as to substantiate the concepts and tools used in it.

2.1 Classification by Sieving

One of the oldest techniques for particle classification — the separation based on the sample size or any other of its physical attributes — and still widely used today is **sieving**. The preponderance of this method is due to some of its advantages, such as low investment cost, relative ease of implementation and execution (which, in turn, requires low technical skills), good reliability and capability to separate particles in sizes that vary from $100mm$ to $0.02mm$ (Kelly and Spottiwood, 1982). This characteristics are usually do not associated with other classification methods.

The series of sieves used in this work was the *U.S. Sieve Series*, which has the following components:

Table 1. Sieves used in the experiments.

U.S. Sieve Series	N^o4	N^o8	N^o12	N^o16	N^o20	N^o30	N^o40
Aperture (mm)	4.750	2.360	1.700	1.180	0.850	0.600	0.425
Mesh	4	8	12	16	20	30	40
U.S. Sieve Series	N^o50	N^o70	N^o100	N^o140	N^o270	N^o400	—
Aperture (mm)	0.300	0.212	0.149	0.106	0.052	0.038	—
Mesh	50	70	100	140	270	400	—

2.2 Image Acquisition

Image capture for processing and analysis was performed by means of a Digital Photo Camera *Canon EOS Digital SLR Camera – Rebel XTi*, of a Trinocular Stereoscopic Microscope *Taimin XTB-1B* and a Table Scanner *Microtek ScanMaker i800*. Using these three devices, four methods of image acquisition were tested: 1. the photographic camera equipped with a 50mm objective; 2. the photographic camera equipped with macro lens; 3. the microscope with a photographic

camera attached to it; and 4. the table scanner.

Being in possession of such equipment and of the ore samples, the next step was to define the useful viewing range for each device and its associations. This range was set from two items: 1. the apparatus physical feasibility; and 2. its visualization (in other words, the field of view in the captured image).

Verify the apparatus physical feasibility consists on checking if it is possible to capture the image of a specific grain size with a certain device or association of devices. For example, it is impossible to use the scanner to capture images of grains larger than 1.5 mm (mesh number 12, 8 and 4) because the lid of the scanner will not closed due to the grain size. On the other hand, the visualization has — as its determining factor — the field of view in the captured image. This field of view is very restricted, for example, in the camera with microscope association. In this case, to capture grains larger than $600\mu m$ (meshes number 30, 20, 16, 12, 8 and 4) involves viewing only a few grains fully contained in the image, reducing the granulometry reliability (Francus, 2005). In Table (2) one can verify the useful particle visualization range. In this table, "P.C. 50*mm*" means the photographic camera with 50*mm* lenses, "P.C. Macro" means the photographic camera with macro lenses e "P.C. + Mic." means the association of the photographic camera with the microscope.

Table 2. Useful particle visualization range.

Mesh	4	8	12	16	20	30	40	50	70	100	140	270	400
P.C. 50*mm*	x	x	x	x	x	x	x						
P.C. Macro					x	x	x	x	x	x	x	x	
P.C. + Mic.							x	x	x	x	x	x	x
Scanner				x	x	x	x	x	x	x	x	x	

2.3 Morphological Operations

To extract components of interest in a digital image is one of the fundamental problems in the image processing and analysis field (Francus, 2005). Regarding the image processing and computer vision, Mathematical Morphology is used as a tool to extract components of an image that are useful in representing and describing its shape, such as borders (or frontiers), circularity, convexity, ellipticity, convex hull and symmetry.

As will be seen next, the main idea of studying Mathematical Morphology is to extract information on the geometry and topology of an unknown set (or ensemble), that is, an image, and compare this information with a well-defined set called **structuring element**. The structuring element has, in general, geometric and/or topological characteristics according to the information to be extracted in the set of interest. The structuring element is a matrix used to define the shape and size of a neighborhood for morphological operations. The structuring element matrix has a binary support (which means that it is composed of 0s and 1s) and can have an arbitrary shape and size which varies according to what is to be analyzed. For example, if the object that is to be extracted from an image has a linear shape, it is appropriate to use linear structuring elements. There are linear, circular and composed structural elements.

Dilation and *erosion* are the most used morphological operators. From them, other morphological operations of greater complexity can be expressed, providing interesting and useful results in image processing. Next there will follow a brief description and definition of the morphological operations used in this work.

2.3.1 Dilatation

Dilation is the process of incorporating to the object all the points of its *surrounding* background, leaving it with a larger area. The dilation is useful to fill gaps or holes between objects in an image.

Definition 1 *Let A and S to be subsets of Z^2. The dilation of the set A by the set S is defined as the operation*

$$A \oplus S = \{x \mid (\hat{S})_x \cap A \neq \emptyset\}, \tag{1}$$

where $\emptyset$ is the empty set and S is the structuring element.

2.3.2 Erosion

Erosion is the process of eliminating an object's border points, leaving it with a smaller area, in pixels. For this reason, the operation of erosion is useful either to remove small objects or to separate objects that are touching in an image.

Definition 2 *Let A and S to be subsets of Z^2. The erosion of the set A by the set S is defined as the operation*

$$A \ominus S = \{x \mid (S)_x \subseteq A\}. \tag{2}$$

2.3.3 Opening

The opening operation is a process composed by an erosion followed by a dilation. Although the two are opposite operations, one does not undo the other and so the result of applying an opening operation depends on the initial image. The effects of a morphological opening in an image are: elimination of small and narrow objects, breaking objects into smaller pieces and, generally, a contour smoothing without a significant change in the image area. For this reason the erosion operation is useful both to remove small objects in a picture as to separate objects that are touching.

Definition 3 *Let A and S to be subsets of Z^2. The morphological opening of the set A by the set S, denoted by $A \circ S$, is the erosion of the set A by the set S followed by a dilation of the result by the set S and is defined as*

$$A \circ S = (A \ominus S) \oplus S. \tag{3}$$

In Figure (1) there is an example of the morphological opening. In this case, the morphological operation aims to eliminate small and imperfect grains. Figure (1a) has a few grain pieces remaining from the processing. The result of a morphological opening with a structuring element in the form of a disk of radius 15 is seen in Fig. (1b), which has only the whole grains, without the small objects from the previous image.

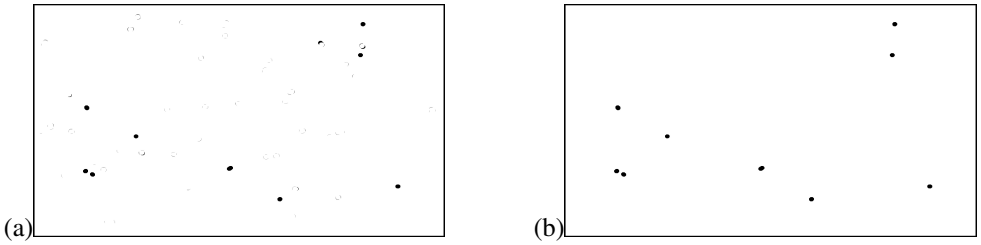

Figure 1. Effect of the opening operation using a disk structuring element with a radius 15: (a) image with pieces of grains; (b) morphological opening processed image.

2.4 Morphological and Physical Sieving

To estimate the relationship between the mass retained in the manual and computer sieving, it was used the equation that relates mass and volume $m = \rho V$, where ρ is the ore's density — or specific mass. As the computational sieving was performed with a disc-shaped structural element, by knowing the number of particles with a given radius r it is possible to approximate the ore weight for that specific particles' area or volume.

Thus, the procedure followed was: 1. Calculating the relationship between the mass of the product obtained by manual sieving; 2. Computational separation followed by counting the grains retained in each computational mesh; 3. Determination of the size of the division between the sieves (the cutting radius) 4. Grain area and volume approximation.

3. RESULTS

This section presents the results concerning the display range of all equipments used in the image acquisition and the Mathematical Morphology sieving. It also compares manual and digital sieving methods. The results of lighting correction in the images captured with the macro lens are shown in Subsection (3.2). As shown before, Tab. (2) gives the useful particle visualization ranges for each image acquisition method used in this work.

3.1 Computational Sieving Using Mathematical Morphology

The processing steps involved in the computational sieving method using Mathematical Morphology will be illustrated based on two example images, each one captured with a different instrument. The first image was captured with a camera equipped with 50*mm* lenses (its standard lenses) and the second one was captured with a scanner. Both images are preprocessed by means of a binarization operation.

For each image, charts with the particle size distribution, histograms representing the number of grains versus the amount of pixels found, and images that show the amount of material withheld in each computational sieving stage are given. In the end, a comparison between the manual and computational sieving is done.

There is also a third example image, captured with a camera equipped with macro lenses, that is shown in order to emphasize illumination correction preprocessing.

Camera with 50*mm* lenses: grains on Fig. (2) are obtained from the junction of ore samples retained in sieves with meshes 12 and 16.

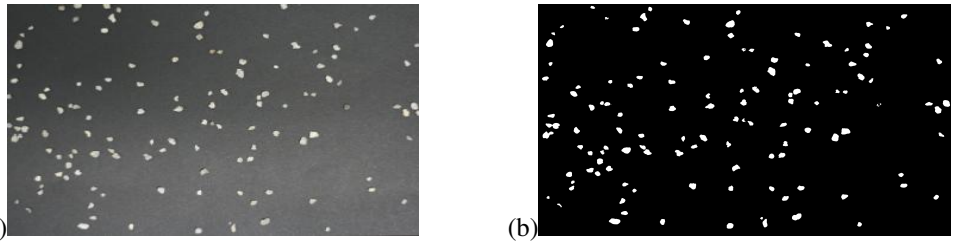

(a) (b)

Figure 2. Junction of sieves with meshes 12 and 16: (a) gray scale image (original); (b) enhanced and binarized image, without objects at the edges.

Figure (3a) represents the computational sieving. Image objects are sifted by opening the image with a structuring element of increasing size and by counting the remaining intensity surface area (the summation of pixel values in the image) after each opening.

In Figure (3b) the first derivative is computed and it is possible to see variations in the number of pixels between two consecutive opening operations. A significant variation between two consecutive opening operations indicates the image has objects of the same size of the structuring element used in the smaller opening operation.

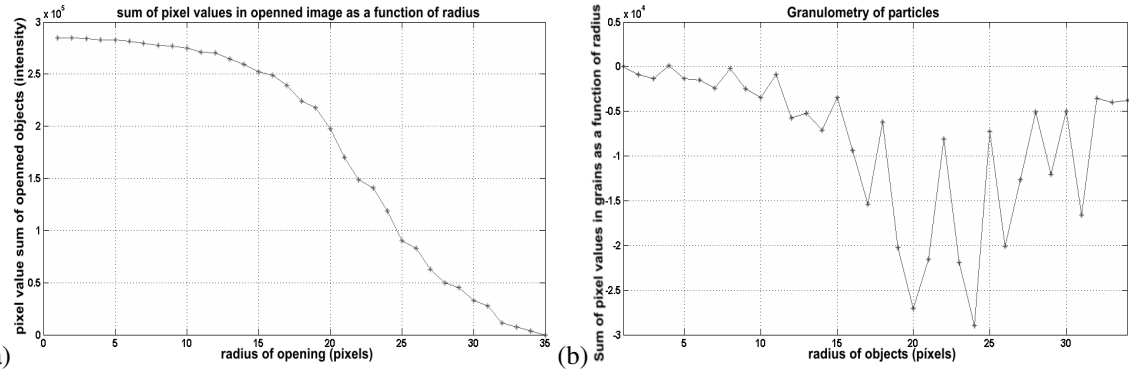

(a) (b)

Figure 3. (a) Computational sieving simulation; (b) Computational variation of grain sizes between sieves.

The histogram shown in Fig. (4) results from the grain counting computational process. Its horizontal axis indicates the number of pixels and its vertical axis represents the amount of grains. According to the computational counting in Fig. (2b) there are 123 grains. Computationally counting the grains agrees with the visual counting. Even grains that are touching each other were separately counted by morphological sieving.

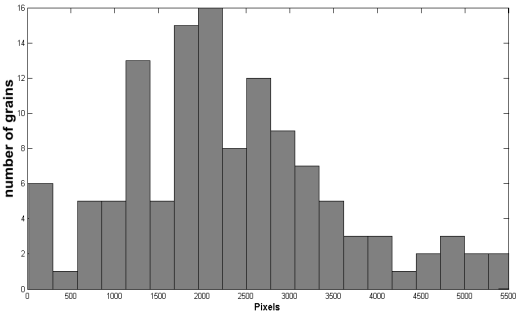

Figure 4. Histogram of grain counting — 123 grains.

Figure (5) displays the result of successive morphological openings as an example of computational sieving. What is seen in (a) is the result of a morphological opening operation with a structuring element of radius 16, in (b) with a structuring element of radius 23 and in (c) with a structuring element of radius 24.

The relationship between manual and computational sieving for the sample in the Fig. (2) is given by the ratio between the masses of the product in sieves 12 and 16, that is:

Ratio between the product mass in the sieves: $\frac{m16}{m12} = \frac{91,71g}{102,16g} \cong 0,9$; Ratio between the estimate of the product mass in the sieves (approximation by their area): $\frac{m16}{m12} = \frac{119,026}{167,605} \cong 0,71$; Ratio between the estimate of the product mass in the sieves (approximation by their volume): $\frac{m16}{m12} = \frac{165,39}{330,836} \cong 0,5$.

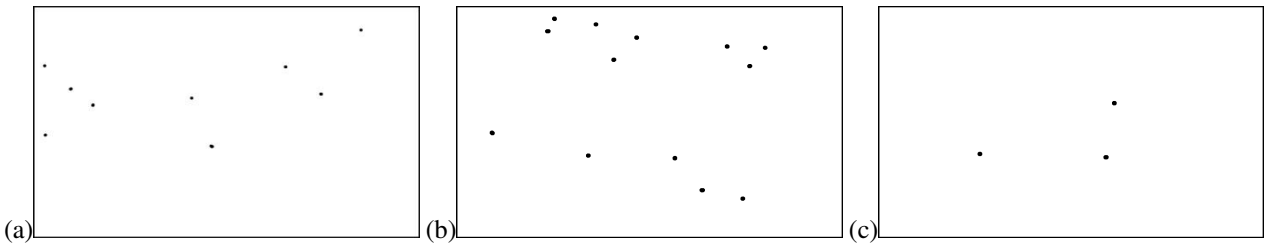

Figure 5. Ore retained in computational sieves. Grains with radius (a) 16, (b) 23, and (c) 24, respectively.

Table 3. Number of particles in each radius of the Fig. (2) — $1mm = 26$ pixels.

Radius (pixels)	11	12	13	14	15	16	17	18	19	20	21
Number of particles	4	2	2	3	4	9	3	10	14	11	4
Radius (pixels)	22	23	24	25	26	27	28	29	30	31	32
Number of particles	9	13	3	8	4	1	4	1	1	1	1

Scanner with 600*dpi* resolution: grains on Fig. (6) are obtained from the junction of ore samples retained in sieves with meshes 40 and 50.

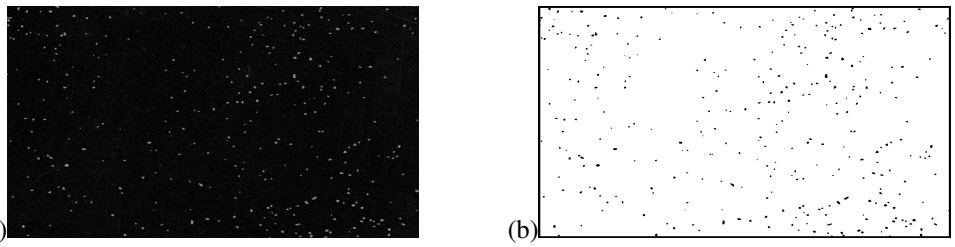

Figure 6. Junction of meshes 40 and 50: (a) gray scale image (original); (b) enhanced and binarized image, without objects at the edges.

The histogram shown in Fig. (7) results from the grain counting computational process. According to the computational counting, in Fig. (6b) there are 319 grains. Again, computationally counting the grains agrees with the visual counting.

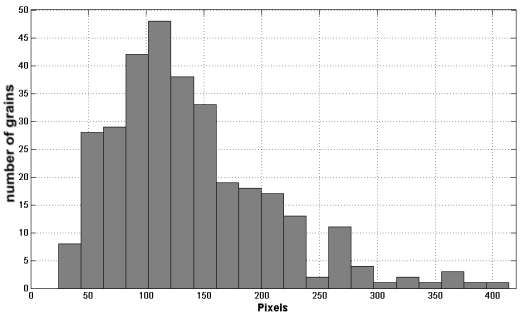

Figure 7. Histogram of grain counting — 319 grains.

The morphological opening operation and the variation in the number of grains between two consecutive opening operations from Fig. (6a) are shown in Figs. (8a) and (8b). In Figure (8a), one can verify that the variation in the structuring element radius was in in a range between three and ten. In Figure (8b) the variation on the amount of remaining grains can be verified.

Figure (9) shows the separation of the grains from Fig. (6a) based on morphological opening and reconstruction operations. In Figure (9i) there are no grains, which means that in this specific image there are no objects with a size bigger than the structuring element of radius 11.

The relationship between manual and computational sieving for the sample in Fig. (6) is given by the ratio between the masses of the product in the sieves 40 and 50, that is:

Ratio between the product mass in the sieves: $\dfrac{m50}{m40} = \dfrac{38,52g}{50,94g} \cong 0,756$; Ratio between the estimate of the product

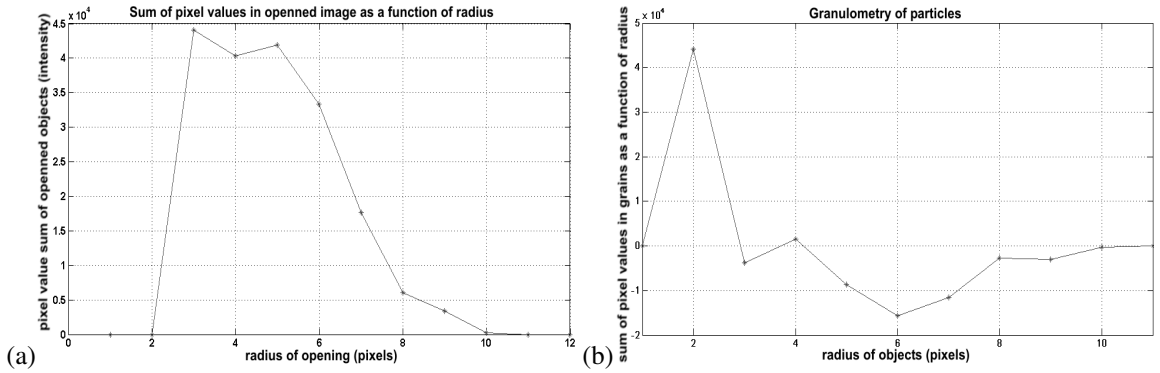

(a) (b)

Figure 8. (a) Opening operation radius in the imagem; (b) Variation of the amount of grains in each opening operation.

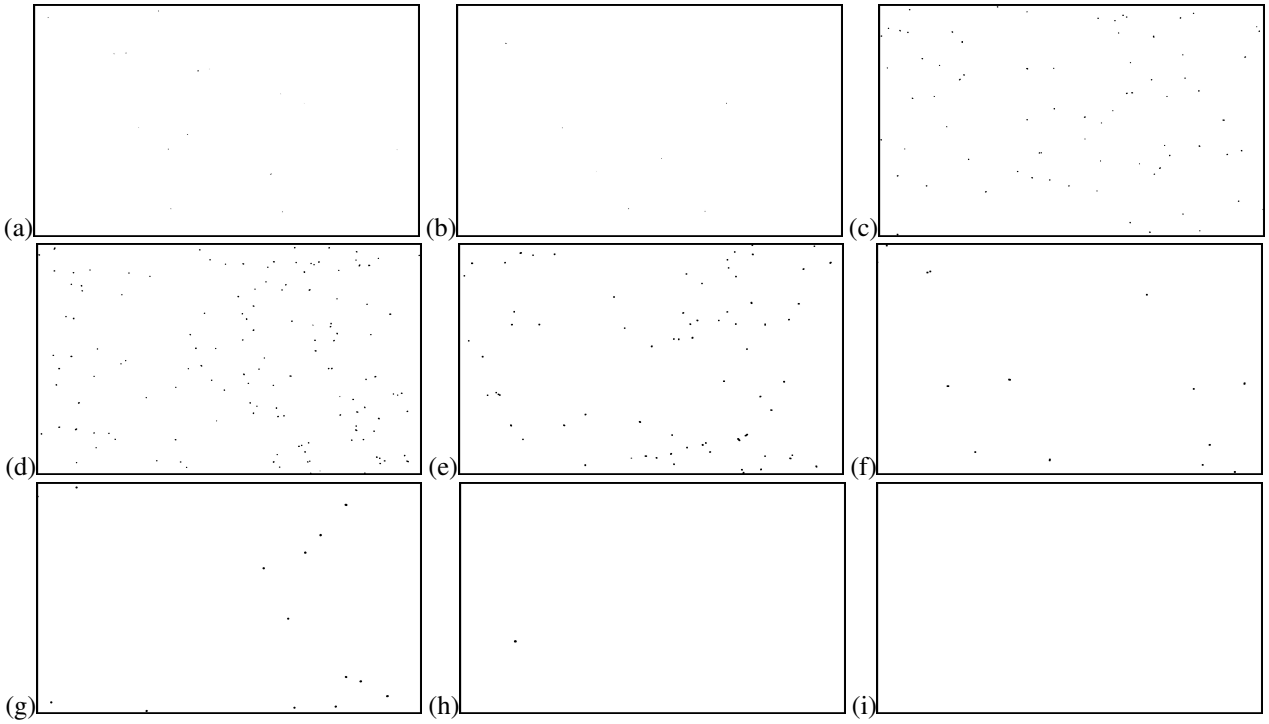

(a) (b) (c) (d) (e) (f) (g) (h) (i)

Figure 9. Ore retained in computational sieves: from (a) to (h) grains with radius from three to ten pixels, respectively; (i) image without grains.

mass in the sieves (approximation by their area): $\frac{m50}{m40} = \frac{8,507}{7,57} \cong 1,124$; Ratio between the estimate of the product mass in the sieves (approximation by their volume): $\frac{m50}{m40} = \frac{1,696}{2,123} \cong 0,799$.

Table 4. Number of particles in each radius of the Fig. (6) — $1mm = 23.62$ pixels.

Radius (pixels)	2	3	4	5	6	7	8	9	10
Number of particles	10	6	74	138	71	14	14	1	0

3.2 Illumination Correction Preprocessing

It is common to use some kind of preprocessing task to correct certain elements in digital images. Illumination correcting is one of those tasks. In the specific case of acquiring an image with a combination of lenses (macro lenses), the images suffer from an effect that makes their edges to shade off gradually, that is, there is a difference in illumination between the center and the edges of the images, as shown in Fig. (10a).

Camera with macro lenses: Figure (10a) represents an ore sample retained in the sieve 140, and Fig. (10b) is its binarized image after the preprocessing stage shown in Fig. (11).

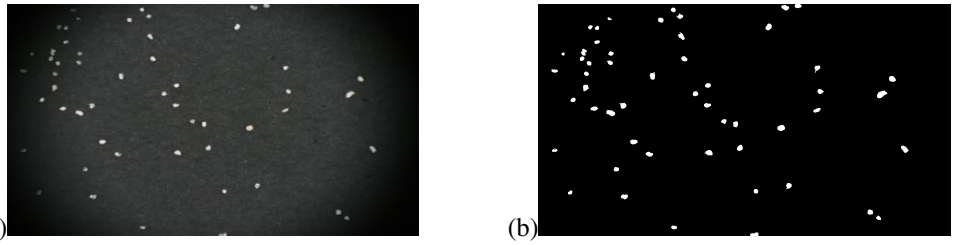

Figure 10. (a) Sample obtained from the sieve 140; (b) Its binarized image.

To correct the illumination in Fig. (10a) a histogram equalization was performed, followed by applying the *imadjust* function in *Matlab*®, which enhances the image. Next, the morphological opening operation is applied using a structuring element with an adequate radius in order to eliminate small objects (the shield noise) that may remain in the image. In the example image shown here, the structuring element used a 12 pixel radius. The result can be seen in Fig. (11). Finally, the image was binarized by adjusting its whitening balance. In this case, a 20% of whitening was used, resulting in what can be seen in the Fig. (10b).

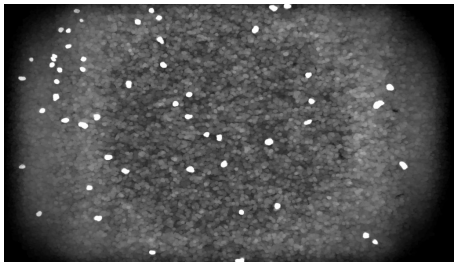

Figure 11. Image Enhancement, histogram equalization and morphological opening on Fig. (10a).

Although these elements were brought together by a single sieve, the computerized method computer identifies different grain sizes. This means that it is possible to operate with "computational sieves" between the values of the physical sieves. The charts shown in Figs. (12a) and (12b) are related to the opening operations and to the grain size variation relatives to the Fig. (10a). It can be seen that from radius 12 there was a sharper decrease in the number of pixels of the image. So from this point one should carry out in the division of the sizes of objects in the image.

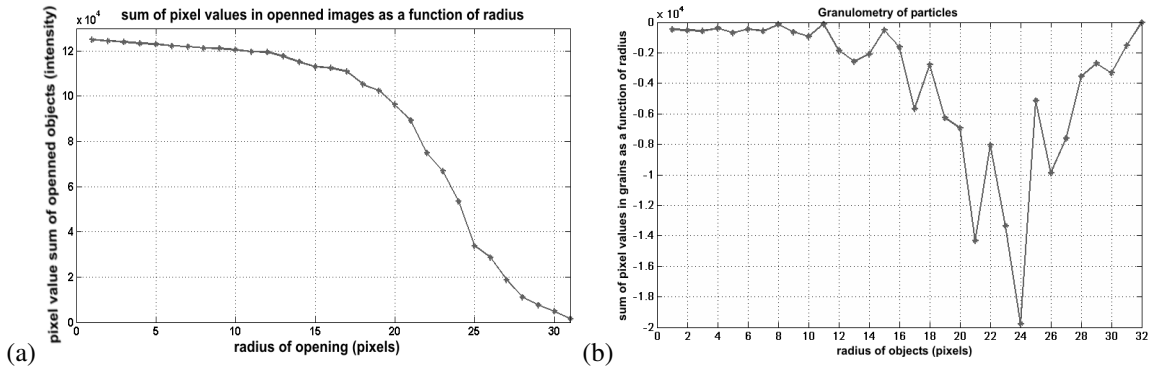

Figure 12. (a) Opening radius in the image; (b) Variation on the amount of grains in each opening.

Figure (13) is the visualization of the number of grains versus the number of pixels (in other words, the grain counting). According to the computational counting, Fig. (10a) shows 52 grains.

4. DISCUSSIONS AND CONCLUSIONS

Computational granulometry by means of Mathematical Morphology shows promising results as it is able to efficiently separate mineral particles of different sizes, as shown in Tab. (2). Comparing the results obtained with morphologic sieving and physical sieving do really presented some discrepancies. This is mainly due to sieving errors and the two dimensional ore image analysis. The ore particles tend to stabilize in the lower energy position, therefore, a simple two dimensional analysis is not sufficient for an accurate prediction. The assumption of spherical particles, common in size profile determination by physical or morphological sieving proved to be inadequate.

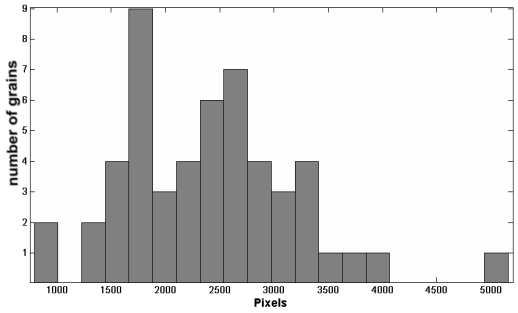

Figure 13. Grain counting histogram — 52 grains.

Regarding to the equipment used, in the case of the camera and microscope association, the useful range extends beyond a 400 *mesh* sieve (in other words, it is possible to capture images with quality in which the grains are smaller than 38 micrometers). The same occurs with the scanner, in which its useful range of view is beyond a 400 *mesh* sieve. However, acquiring images by means of the scanner was difficult because it was necessary to protect it from the ore particles so there was no damage to the device (thus, in this case the particles were arranged on a transparency over the scanner glass). With meshes up to 270, the images were satisfactory, but when 400 *mesh* was reached, the captured images were also showing the imperfections in the plastic, giving an appearance of an image without focus. This does not occur, or at least was not perceived below 270 *mesh*.

Concluding, the results show in this paper stated that even when it is necessary to separate elements trapped in a same sieve, the computational method is able to identify different grain sizes. This means that it is possible to "enter different computer sieves" between the physical mesh values. This is of great importance when there is a need for greater accuracy in the analysis.

5. ACKNOWLEDGEMENTS

The authors wish to acknowledge CNPq for the financial support.

6. REFERENCES

Dur, J. C. and Elsass, F. and Chaplain, V. and Tessier, D. "The relationship between particle-size distribution by laser granulometry and image analysis by transmission electron microscopy in a soil clay fraction", European Journal of Soil Science, pp. 265–270, v. 55, n. 2, 2004.

Francus, P. (Ed.) "Image Analysis, Sediments and Paleoenvironments (Developments in Paleoenvironmental Research Series)" , v. 7, Kluwer Academic Publishers, Dordrecht, 1984.

Kapur, P. C. and Meloy, T. P. "Spirals Observed", International Journal of Mineral Processing, v. 53, nn. 1–2, pp. 15-28, 1998.

Kelly, E. G. and Spottiwood, D. J. "Introduction to mineral processing", Johns Wiley & Sons Inc., New York, 1982.

Kohmuench, J. N. "Improving Efficiencies in Water-Based Separators Using Mathematical Analysis Tools", PhD Thesis, Virginia Polytechnic Institute and State University, 2000.

Lira, B. B. "Simulation of the Woodlawn Grinding Circuit", JKMRC University of Queensland, Australia, 1985.

Lira, B. B. "Modelos Matemáticos De Moagem: Parâmetros e Aplicação", XIV Encontro Nacional de Tratamento de Minérios e Hidrometalurgia, Salvador – BA, v. 1, pp. 546–562, 1990.

Lynch, A. J. and Rao, T. C. "Modeling and Scale-Up of Hydrocyclone Classifiers", Paper No. 9, 11th International Mineral Processing Congress, Cagliari, Italy, v. 1, pp. 546–562, April 21-26, 1975.

Image Processing Toolbox 6.3, "Granulometry of Snowflakes", http://www.mathworks.com/products/image/demos.html ?file=/products/demos/shipping/images/ipexsnow.html. Acessed: April, 2007.

Silva, E. M. da and Lima, J. E. F. W. and Rodrigues, L. N. and Azevedo, J. A. de. "Comparação de modelos matemáticos para o traçado de curvas granulométricas", Pesquisa Agropecuária Brasileira, Brasília, v. 39, n. 4, pp. 363–370, 2004.

Wojnar, L. "Image Analysis – Applications in Materials Engineering", CRC Press, 1999.